Heliyon 8 (2022) e11632

Contents lists available at ScienceDirect

Heliyon

journal homepage: www.cell.com/heliyon

Research article

# Exposure to metal nanoparticles changes zeta potentials of *Rhodococcus* cells

Maria S. Kuyukina [a,b,*], Marina V. Makarova [a], Olga N. Pistsova [a], Grigorii G. Glebov [a,b], Mikhail A. Osipenko [c], Irena B. Ivshina [a,b]

[a] *Microbiology and Immunology Department, Perm State University, Perm, Russia*
[b] *Institute of Ecology and Genetics of Microorganisms, Perm Federal Research Center, Russian Academy of Sciences, Perm, Russia*
[c] *Applied Mathematics and Mechanics Faculty, Perm National Research Polytechnic University, Perm, Russia*

## HIGHLIGHTS

- Nanoparticles (NPs) of transition metals affect *Rhodococcus* viability and zeta potentials.
- Cellular zeta potentials approach the NPs values, suggesting their accumulation on the cell surface.
- More toxic nanometals accumulate stronger on bacterial cell surfaces.
- Cu and CuO NPs increase *Rhodococcus* adhesion to hydrocarbon, but $Fe_3O_4$ NPs reduced the adhesive activity.
- Targeted modification of bacterial cell surface with metal NPs is possible.

## GRAPHICAL ABSTRACT

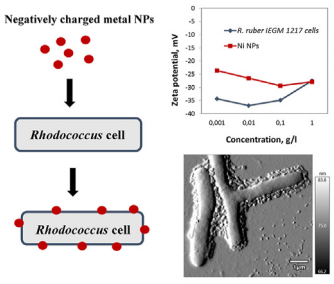


## ARTICLE INFO

*Keywords:*
Metal nanoparticles
Actinobacteria
*Rhodococcus*
Zeta potential
Adhesion
Hydrophobicity

## ABSTRACT

Nanoparticles (NPs) of transition metals and their oxides are widely used in industries and exhibit diverse biological activities – from antimicrobial to growth promoting and regulating biofilms. In this study, the concentration-dependent effects of negatively charged metal and metal oxide NPs on the viability and net surface charge of *Rhodococcus* cells were revealed. Our hypothesis that zeta potential values of bacterial cells approach the zeta potential of NPs with an increase in the concentration of nanoparticles was statistically validated, thus suggesting the accumulation of nanoparticles on the cell surface. Thus, based on the dynamics of zeta potential, it would be possible to predict the accumulation of metal NPs on the cell surface of particular *Rhodococcus* species. It seemed that more toxic nanometals (e.g. CuO) accumulate more intensively on the bacterial cell wall than less toxic nanometals (Bi, Ni and Co). Physical properties of NPs, such as shape, size, dispersity and zeta potential, were characterized at different nanoparticle concentrations, in order to explain their diverse effects on bacterial viability, cellular charge and adhesion to hydrocarbons. Interestingly, an increase in *Rhodococcus* adhesion to *n*-hexadecane was observed in the presence of Cu and CuO NPs, while treatment with $Fe_3O_4$ NPs resulted in a decrease in the adhesive activity. The obtained data help to clarify the mechanisms of nano-bio interaction and make it possible to select metal and metal oxide nanoparticles to modify the surface of bacterial cells without toxic effects.

* Corresponding author.
*E-mail address:* kuyukina@iegm.ru (M.S. Kuyukina).

https://doi.org/10.1016/j.heliyon.2022.e11632
Received 7 April 2022; Received in revised form 19 April 2022; Accepted 10 November 2022

## 1. Introduction

Nanoparticles (NPs) of transition metals and their oxides are widely used in medicine and high-tech industries, such as electronics, optics, information technologies, pharmaceuticals and cosmetics. Due to large specific surface area, adsorption activity, tendency to aggregate and accumulate, high reactivity and catalytic ability, metal NPs exhibit diverse biological activities – from antimicrobial and anticancer to antioxidant and growth promoting [1, 2]. It is important to note the growing role of NPs in environmental protection. For example, nano-chlorapatite immobilized up to 94.13% of leached lead [3]. However, the use of metal nanoparticles is also a cause of allergic reactions. The most pronounced allergic inflammation occurred in mice when exposed to silver and nickel nanoparticles, while gold and silicon dioxide nanoparticles did not cause allergies [4]. There is an important knowledge gap regarding the mechanisms of nanometal interactions with biological systems and toxic effects of NPs greatly dependent on their physicochemical properties (size and shape, surface free energy and

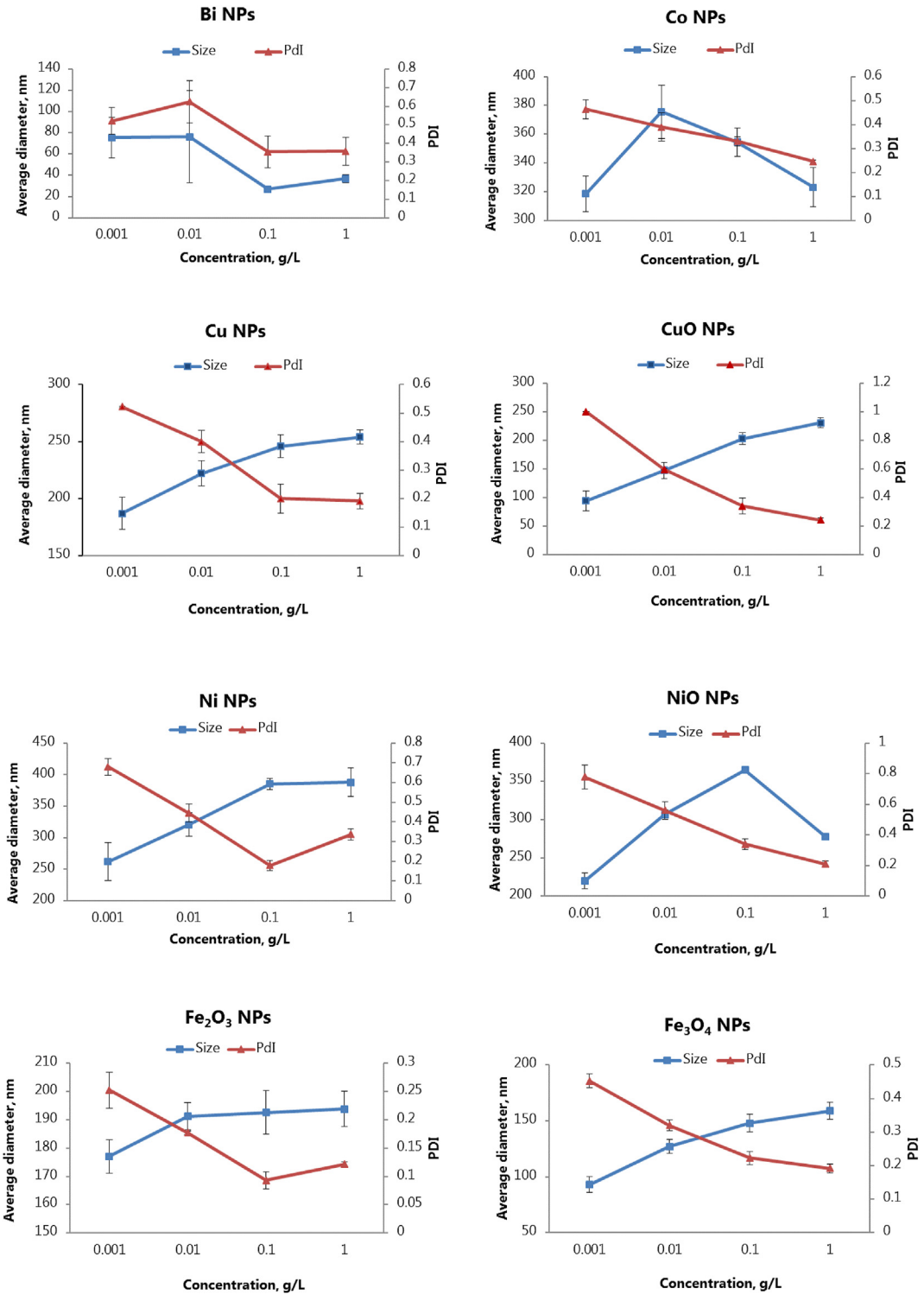


**Figure 1.** Size and PDI values of metal nanoparticles determined by dynamic light scattering, depending on the concentration of NPs.

charge, zeta potential and chemical composition) and particle concentrations [5]. For example, Xu et al. [6] studied the influence of cerium oxide NPs on bacterial biofilm formation, and the main conclusion drawn from NP exposure experiments was that low levels of $CeO_2$ $NP_S$ (<4 mg/L) significantly increased biofilm formation and the growth of individual bacterial cells, while concentrations above 10 mg/L had an inhibitory effect. The zeta potential, reflecting the electrostatic interactions between dispersed particles and a measure of the effective electric charge on the nanoparticle's surface, is a key feature of NPs that governs their biological activity, in particular, their binding to the cell surface and internalization [5, 7].

The surface charge of bacteria, usually negative, is the result of the ionization of carboxyl, phosphate or amino groups and the adsorption of ions from the medium. In addition, macromolecules present in the cell wall and membranes, such as proteins, phospholipids, teichoic acids, teichuronic acids and lipopolysaccharides, also contribute to the net surface charge. According to our previous and other studies, the zeta potential plays an important role in bacterial aggregation and adhesion to hydrocarbon-water interfaces and solid surfaces, and can also provide useful information about the viability and cell surface permeability under stress [8, 9, 10].

While both Gram-positive and negative bacteria have a negatively charged cell wall, Gram-positive bacteria are considered more resistant to metal NPs, presumably due to thicker peptidoglycan layer acting as a protective barrier [11]. Positively charged metal NPs bind to negatively charged peptidoglycan and teichoic acids on the surface of Gram-positive

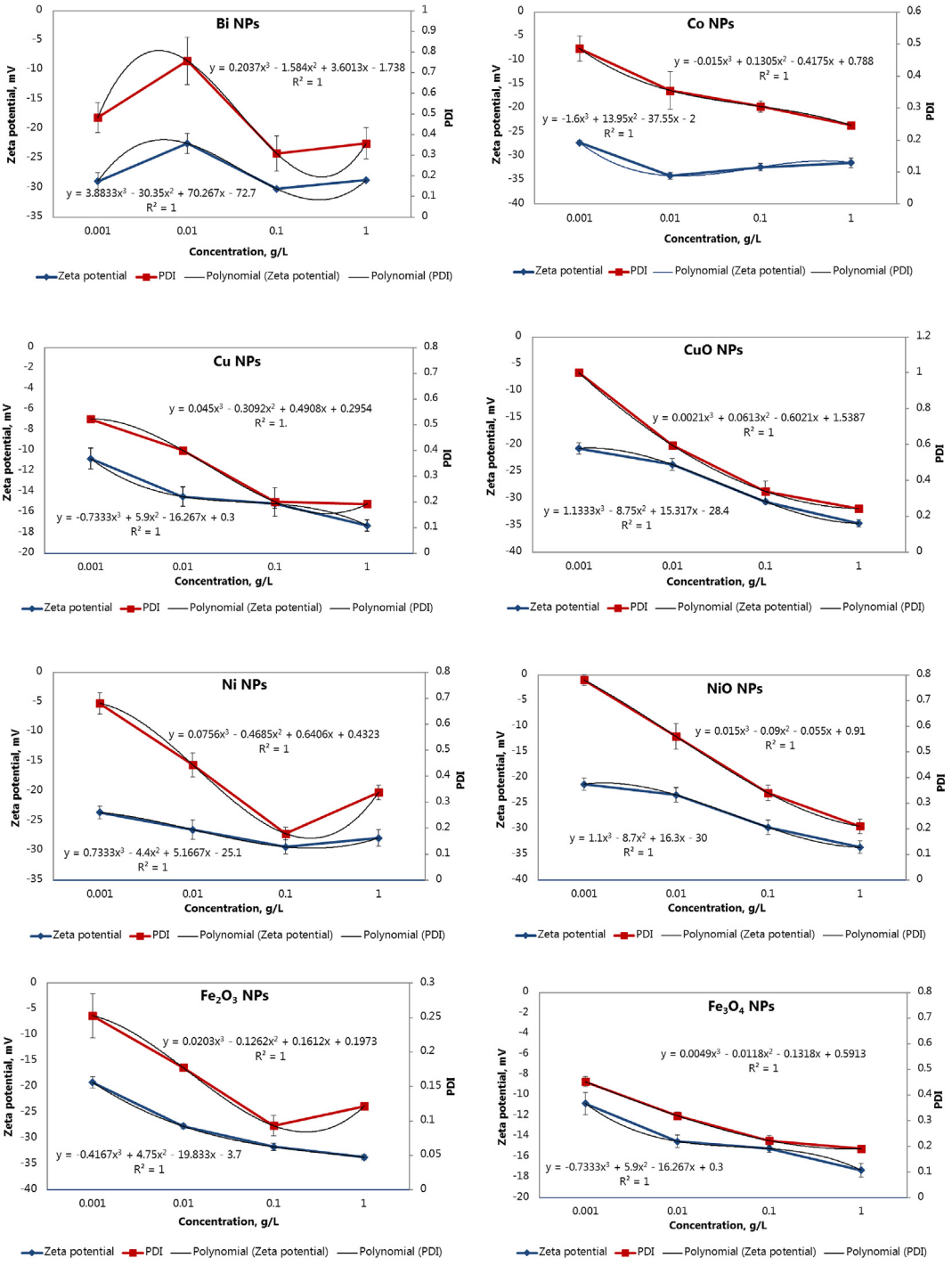


**Figure 2.** Correlation between zeta potential and PDI values of metal NPs depending on their concentrations.

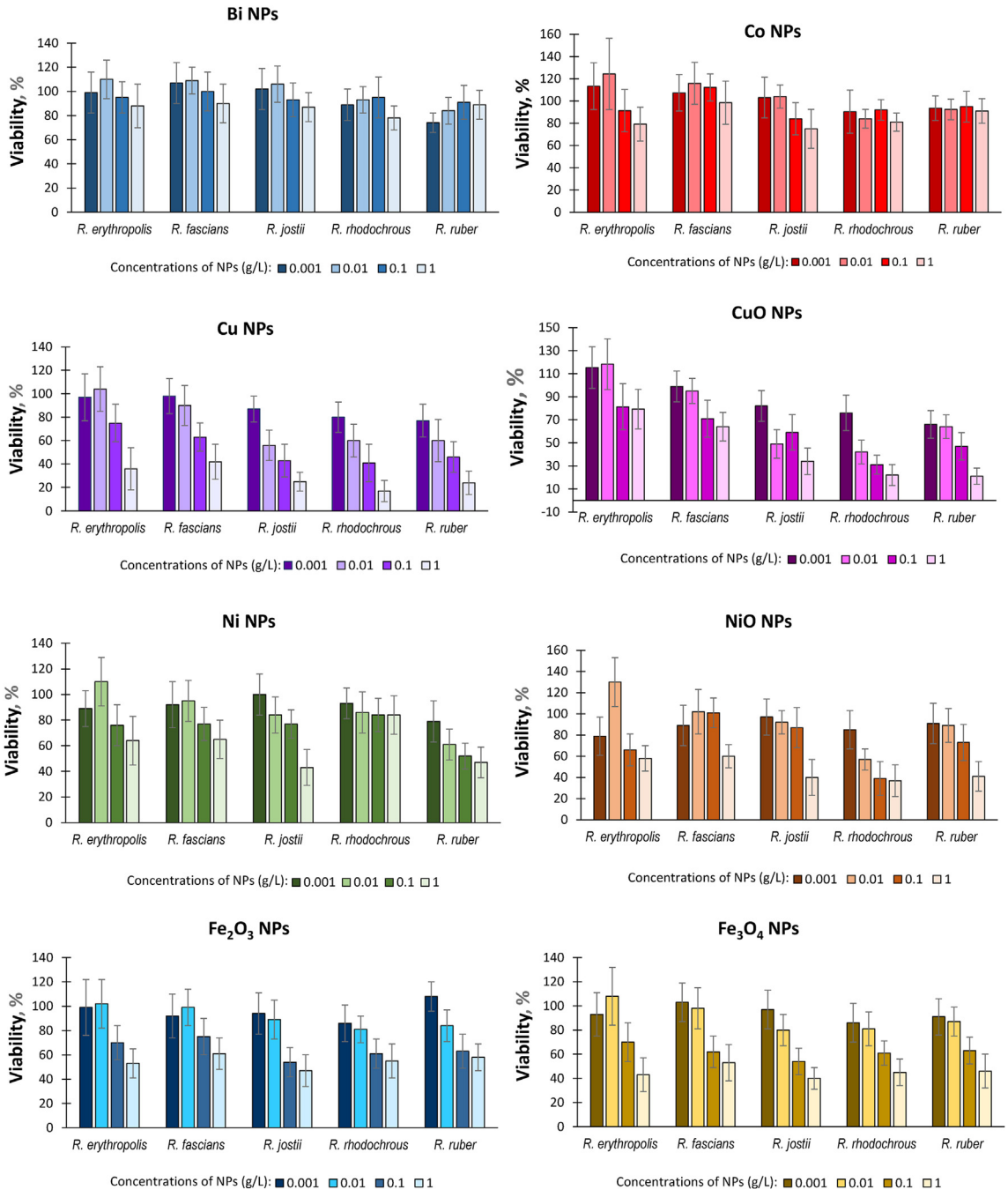


**Figure 3.** Effects of metal NPs on the viability of *Rhodococcus* cells (mean values for each *Rhodococcus* species are shown).

bacteria, thus altering the zeta potential of cells [12]. Cationic nanometals, interacting with the bacterial membrane, increase the production of reactive oxygen species and have a mechanical effect on the membrane, which leads to the depolarization of the membrane and cell damage. For example, chemically synthesized ZnO NPs with a positive zeta potential showed high antimicrobial activity at minimum inhibitory concentrations of 50 and 100 mg/L for Gram-negative and positive bacteria, respectively [13]. Alternatively, ZnO NPs modified with sodium citrate to gain a negative zeta potential had low antibacterial activity. Silver NPs synthesized using an aqueous extract of *Rosa brunonii* Lindl had a negative charge ($-34 \pm 0.95$ mV) and exhibited moderate antimicrobial activity against *Campylobacter jejunii* and *Aspergillus niger* [14].

Interestingly, the zeta potential of negatively charged bacterial cells has moved to neutral upon the incubation with increasing concentrations of positively charged ZnO NPs, while such effect was insignificant for negatively charged ZnO NPs [13]. Generally, much less is known about the interaction of negatively charged nanoparticles with bacterial cells. Since bacterial cells have a negative net charge, there would be repulsive interactions between similarly charged surfaces, while some other nano-bio interface mechanisms may occur, such as hydrophobic, hydrogen-bonding, ligand-receptor, Van der Waals and ionic interactions [15]. Apart from antibacterial effects, nanoparticles can be used for the cell surface engineering that should also include strategies compatible with cell viability and reducing the NP internalization by cells [16].

Actinobacteria of the genus *Rhodococcus* are valuable bioremediation agents degrading a range of harmful and recalcitrant chemicals, such as petroleum hydrocarbons, phenols, solvents, pesticides and pharmaceutical pollutants [17]. Rhodococci are also able to sequester heavy metal

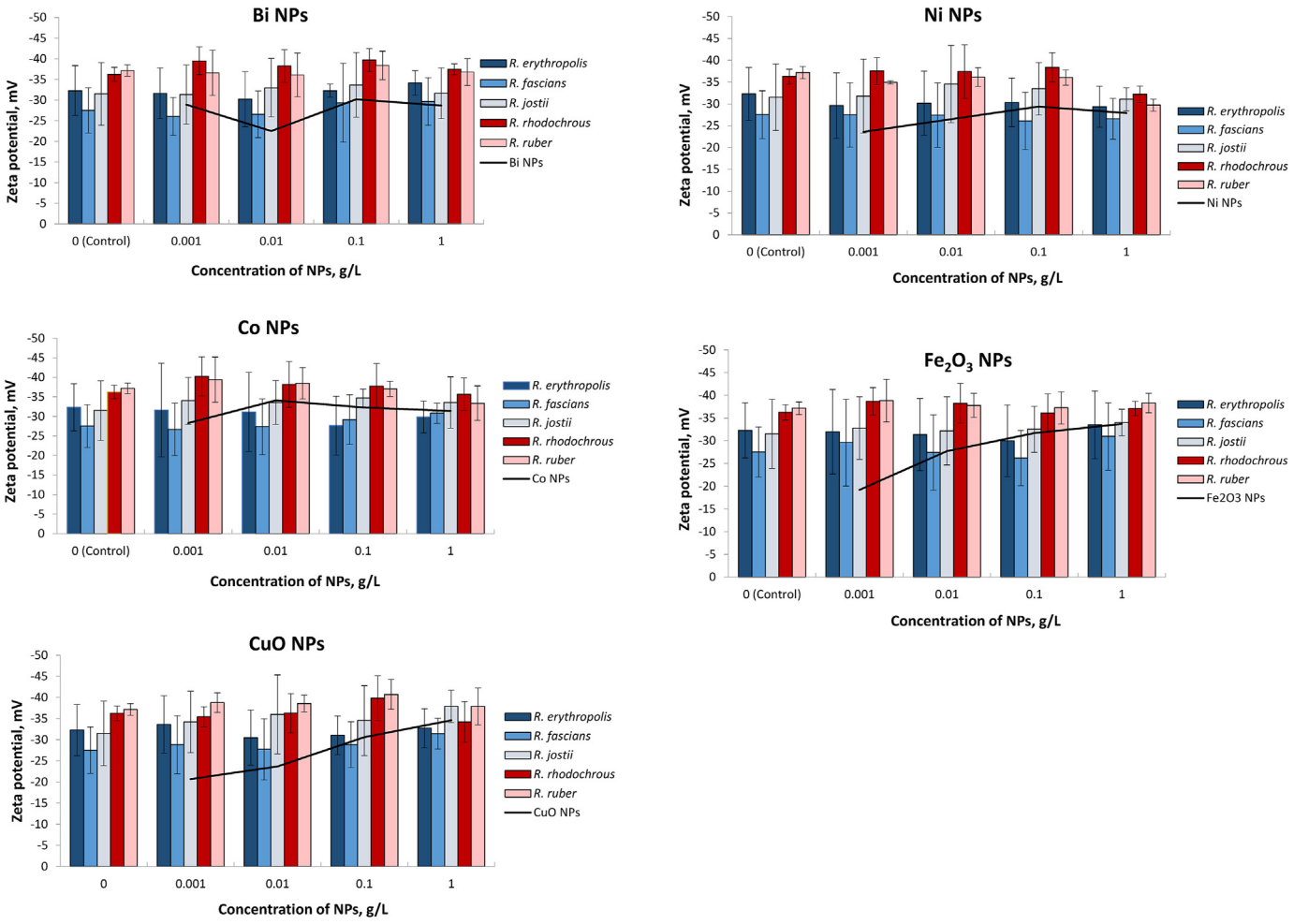


**Figure 4.** Changes in the cellular charge (zeta potential) of *Rhodococcus* at different concentrations of metal NPs.

ions by biosorption and active accumulation, while the study of their interaction with metal nanoparticles is just beginning, and further research is needed to understand the structural and functional modifications of the cell surface with nanometals [18].

This study is aimed at investigating the concentration-dependent effects of negatively charged metal NPs on the net surface charge of *Rhodococcus* cells and statistically testing the hypothesis that zeta potential values of bacterial cells approach the zeta potential of NPs with an increase in the concentration of nanoparticles. It was assumed that the use of 8 different metal and metal oxide NPs in 10-fold concentrations and 25 strains belonging to five *Rhodococcus* species would provide a sufficient data volume for statistical analysis. Also, physical properties of NPs, such as size (hydrodynamic diameter), PDI and zeta potential, were characterized at different nanoparticle concentrations, trying to explain their diverse effects on bacterial viability, cellular charge and adhesion to hydrocarbons.

## 2. Materials and methods

### 2.1. Metal nanoparticles

The nanoparticles of Bi, Co, Cu, CuO, Ni, NiO, $Fe_2O_3$ and $Fe_3O_4$ in an aqueous solution stabilized with 0.1% β-cyclodextrin were purchased from M9, Tolyatti, Russia (http://en.nmt-9.com/). NPs were used in tenfold concentrations (0.001–1.0 g/L). Immediately before the measurement, NPs were washed twice with 10 mM $KNO_3$ (pH 5.5–6) to remove β-cyclodextrin and dispersed for 2 min using a Soniprep 150 (MSE, UK) ultrasonic homogenizer.

### 2.2. Bacterial cultures and growth conditions

Bacterial strains used were the members of different *Rhodococcus* species, namely *R. erythropolis* IEGM 344, IEGM 661, IEGM 693, IEGM 706, IEGM 766, *R. fascians* IEGM 173, IEGM 525, IEGM 531, IEGM 534, IEGM 1218, *R. jostii* IEGM 60, IEGM 68, IEGM 458, IEGM 508, IEGM 550, *R. rhodochrous* IEGM 757, IEGM 1161, IEGM 1162, IEGM 1360, IEGM 1362, *R. ruber* IEGM 628, IEGM 1121, IEGM 1135, IEGM 1217, IEGM 1352 from the Regional Specialized Collection of Alkanotrophic Microorganisms of the Institute of Ecology and Genetics of Microorganisms, Perm, Russia (IEGM; www.iegmcol.ru; WFCC/WDCM 768; UNU/CKP 73559/480868). Bacteria grown on nutrient agar were harvested, washed twice and suspended in 10 mM $KNO_3$ to an optical density ($OD_{600}$) of 0.5.

### 2.3. Atomic force microscopy of nanoparticles and bacterial cells

The shape, sizes and surface roughness of metal NPs were determined by atomic force microscopy (AFM) with the MFP-3D-BIO (Asylum Research, USA) atomic force microscope using tapping mode in air. Approximately 10 μl of freshly sonicated NP suspensions (0.01–0.1 g/L) were deposited on a cover glass and allowed to dry. Images were acquired using Olympus AC240TS silicon cantilevers with resonance frequencies of 50–90 kHz and spring constants of 0.5–4.4 N/m and processed using the Igor Pro 6.22A (WaveMetrics, USA) software. The dimensions (length and width) and root mean square (RMS) roughness of NPs were calculated from the height images. Minimum 50 NPs of each variant were scanned and calculated.

AFM images of *Rhodococcus* cells incubated with metal NPs were obtained under the same conditions.

### 2.4. Measurements of size and polydispersity index (PDI) of nanoparticles

The hydrodynamic diameters and PDI of nanoparticles were measured by dynamic light scattering at an angle of 173 or 90° using a ZetaSizer Nano ZS (Malvern Instruments, UK) analyzer. The principle of this method is to measure and analyze fluctuations in the intensity of scattered light in a solution containing colloidal particles [19]. The fluctuations of the scattered light intensity correspond to the velocities of constant thermal motion (Brownian motion), in which the colloidal particles are located. The speed of Brownian motion is related to particle size: smaller particles move faster than larger particles. The range of colloidal particle sizes measured by dynamic light scattering using the ZetaSizer Nano ZS analyzer is quite wide, from 0.6 nm to 6 microns, which fits the sizes of metal NPs but not *Rhodococcus* cells [19].

Polydispersity index (PDI) of metal NPs was determined as $2c/b^2$, where b is the average hydrodynamic (Z–average) diffusion coefficient, and c is the viscosity coefficient of the dispersant. The calculations of average hydrodynamic particle sizes and the measurement of the size distribution are defined by the International Standard ISO 22412: 2017. It should be noted that for samples with PDI over 0.5, the Z-average size mean is inappropriate and a distribution analysis was used to determine the peak positions [20]. All measurements were performed in 3 parallel replications.

### 2.5. Measurements of the zeta potential of bacterial cells and nanoparticles

A ZetaSizer Nano ZS analyzer (Malvern Instruments, UK) was used to measure the electrokinetic (zeta) potential of metal NPs and bacterial cells by electrophoretic light scattering. The electrophoretic mobility was obtained by performing an electrophoresis experiment on the sample and measuring the velocity of the particles using the laser Doppler velocimetry [19, 20]. The sample was placed in a cuvette with a submersible electrode, to which an electric field was applied, which led to the movement of particles to the oppositely charged electrode at a rate proportional to the field strength and the charge of cells or nanoparticles. The calculation of zeta potential from the electrophoretic mobility was performed applying the Henry equation using a Smoluchowski model, which fits for particles larger than 0.2 microns dispersed in electrolytes containing more than $10^{-3}$ molar salt [19]. All measurements were performed in 3 parallel replications.

### 2.6. Bacterial viability and adhesive activity under the exposure to nanoparticles

Metal NP impact on *Rhodococcus* cell viability was evaluated using the modified iodonitrotetrazolium (INT) staining method [21]. For this, bacteria were incubated with various NP concentrations in 96-well microplates, then 0.1 % (w/v) INT solution was added for 24 h, thus allowing the reduction of INT into insoluble red–violet INT-formazan, which concentration was measured spectrophotometrically using a microplate reader (Multiskan Ascent, Thermo, Finland) at 630 nm ($OD_{630}$) in 8-fold replications. Cell viability (%) was calculated compared to corresponding positive control (without NPs) suspensions.

The adhesion of control and treated with metal NPs *Rhodococcus* cells to *n*-hexadecane (98%, Vekton, Russia) was determined in the Microbial Adhesion to Hydrocarbons (MATH) test according to a modified method [9]. All measurements were performed in 3 parallel replications.

### 2.7. Statistics and mathematical modeling

Experimental data were statistically analyzed using a standard Excel program, calculating the mean and standard deviation (m ± SD), shown in figures as SD bars. In addition, data on the zeta potential of bacterial cells and metal NPs depending on the concentration of nanoparticles were processed using the method of least squares according to the linear dependence.

## 3. Results and discussion

### 3.1. Size, polydispersity and zeta potential of metal NPs

AFM imaging revealed different forms and dimensions (ranging from 150 to 350 nm) of metal and metal oxide NPs suspended in water, as well as 0.5–1.5 micron-size aggregates produced by most NPs, namely Ni, Co, CuO, NiO and $Fe_2O_3$ (Supplementary material, Table S1). Data on surface roughness indicated that aggregates generally had higher RMS roughness values compared to single NPs, except for Ni and NiO NPs having the same roughness in dispersed and aggregate state.

The AFM results were mostly in agreement with the data on NP hydrodynamic diameters obtained by dynamic light scattering (Figure 1). The following average size parameters of NPs were determined in ascending order: Bi – 60 ± 35, $Fe_3O_4$ – 126 ± 33, CuO – 175 ± 54, Cu – 184 ± 16, $Fe_2O_3$ – 189 ± 9, NiO – 206 ± 12, Ni – 339 ± 62, Co – 343 ± 27 nm. Moreover, for NPs of a smaller size (Bi, $Fe_3O_4$ and CuO), higher standard deviations were characteristic probably due to more intense aggregation at higher concentrations.

A concentration-dependent relationship between size and PDI values of metal NPs determined by dynamic light scattering was revealed. According to Figure 1, the hydrodynamic diameters of metal NPs strongly depended on their concentrations. Namely, the sizes of Ni, Cu, CuO, $Fe_2O_3$ and $Fe_3O_4$ NPs increased monotonously with the concentration increase, while this value unevenly decreased for the smallest Bi NPs and first increased and then decreased almost to the original value for Co and

**Table 1.** Degree of hypothesis confirmation for studied *Rhodococcus* spp. strains and metal NPs.

| *R. erythropolis* | Bi NPs | $Fe_2O_3$ NPs | Ni NPs | Co NPs | CuO NPs |
|---|---|---|---|---|---|
| IEGM 344 | 0 | 3 | 0 | 2 | 2 |
| IEGM 661 | 2 | 3 | 3 | 3 | 3 |
| IEGM 693 | 1 | 3 | 3 | 2 | 3 |
| IEGM 706 | 2 | 3 | 3 | 2 | 3 |
| IEGM 766 | 2 | 0 | 1 | 2 | 3 |
| *R. fascians* | | | | | |
| IEGM 173 | 1 | 3 | 3 | 3 | 3 |
| IEGM 525 | 2 | 0 | 1 | 2 | 0 |
| IEGM 531 | 0 | 3 | 3 | 3 | 3 |
| IEGM 534 | 3 | 0 | 1 | 3 | 3 |
| IEGM 1218 | 1 | 0 | 0 | 3 | 0 |
| *R. jostii* | | | | | |
| IEGM 60 | 1 | 3 | 3 | 2 | 3 |
| IEGM 68 | 2 | 3 | 3 | 3 | 3 |
| IEGM 458 | 1 | 3 | 3 | 1 | 2 |
| IEGM 508 | 2 | 3 | 3 | 2 | 3 |
| IEGM 550 | 2 | 3 | 2 | 2 | 3 |
| *R. rhodochrous* | | | | | |
| IEGM 757 | 2 | 3 | 3 | 1 | 3 |
| IEGM 1161 | 2 | 3 | 3 | 3 | 3 |
| IEGM 1162 | 2 | 3 | 3 | 3 | 3 |
| IEGM 1360 | 3 | 3 | 3 | 3 | 3 |
| IEGM 1362 | 2 | 3 | 3 | 3 | 3 |
| *R. ruber* | | | | | |
| IEGM 628 | 3 | 3 | 3 | 3 | 3 |
| IEGM 1121 | 2 | 3 | 3 | 3 | 3 |
| IEGM 1135 | 1 | 3 | 3 | 2 | 3 |
| IEGM 1217 | 0 | 3 | 3 | 3 | 3 |
| IEGM 1352 | 2 | 3 | 3 | 3 | 3 |

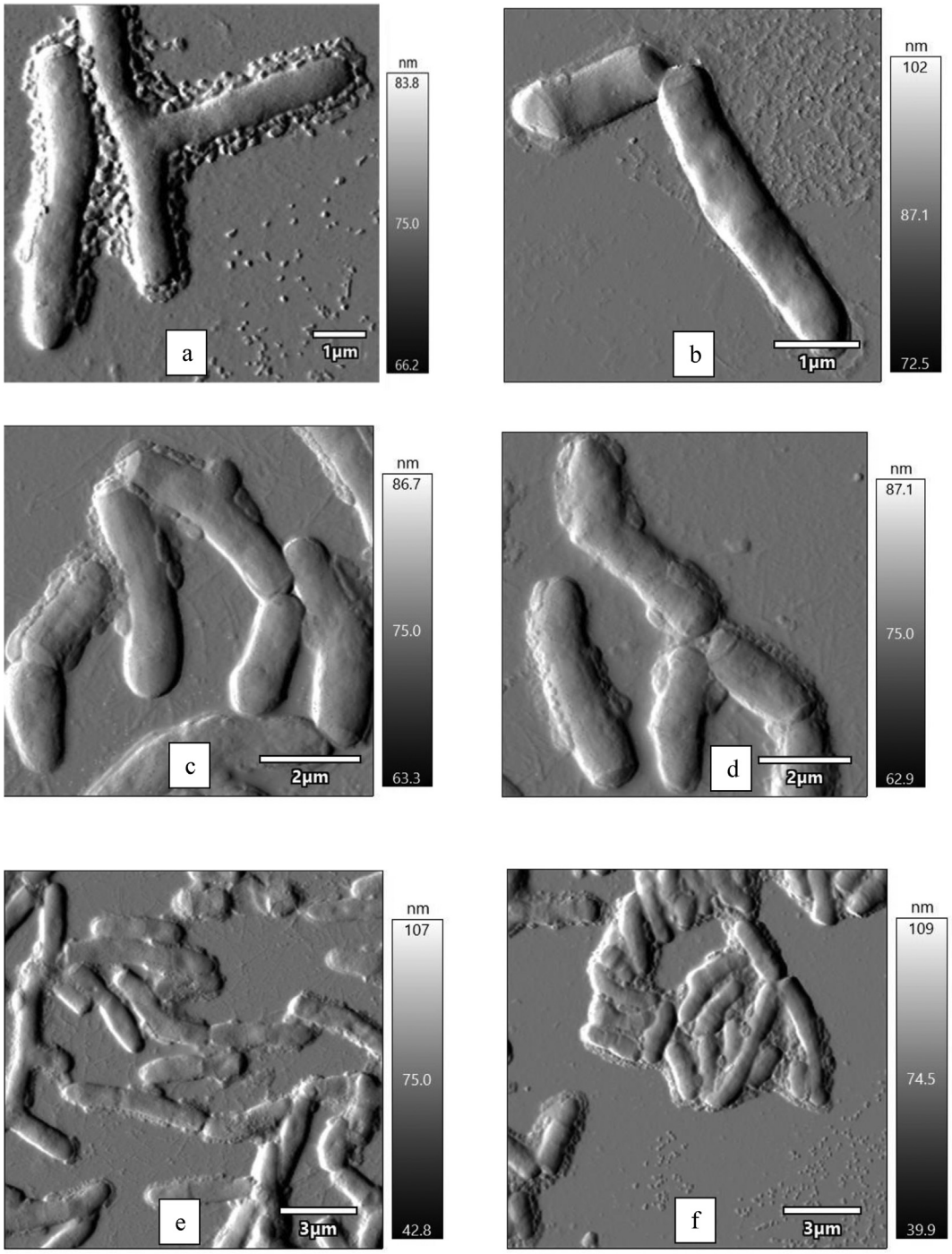


**Figure 5.** AFM images of *Rhodococcus* cells incubated in the presence of metal NPs: *R. rhodochrous* IEGM 1363 with CuO NPs (a); *R. jostii* IEGM 458 with Ni NPs (b); *R. ruber* IEGM 628 with $Fe_3O_4$ NPs (c); *R. ruber* IEGM 628 with NiO NPs (d); *R. erythropolis* IEGM IEGM 693 with Co NPs (e); *R. rhodochrous* IEGM 1161 with Bi NPs (f).

NiO NPs. Such variable concentration-dependent size dynamics contrasted with a steady decline in PDI values revealed for all NPs, showing that more concentrated NP suspensions were more homogenous, with threshold concentrations (0.001 g/L for $Fe_2O_3$, $Fe_3O_4$, Co, Bi, and 0.01 g/L for Ni, NiO, Cu and CuO NPs) where PDI $\leq$ 0.5 that allowed appropriate dynamic light scattering measurements. It should be noted that the aggregation of NPs, registered as the second peak on size distribution graphs (Supplementary material, Figure S1) corresponding to a larger hydrodynamic diameter (around 1000 nm), was observed generally at concentrations $\geq$ 0.1 g/L.

Zeta potentials of all metal NPs measured by electrophoretic light scattering were negative, ranging from −19 to −36 mV under the experimental conditions (10 mM $KNO_3$, pH 5.5–6). The zeta potential values of metal NPs also depended on their concentrations and moved to higher negative values with an increase in the concentration of NPs. A strong positive correlation was found between zeta potential and PDI values (Figure 2), showing that at higher (>0.01–0.1 g/L) concentrations, metal NPs formed relatively monodisperse suspensions (with PDI $\leq$ 0.5) and had zeta potentials close or higher −30 mV, thus indicating their good stability in aqueous systems, suitable for potential biological applications [22].

**Table 2.** Correlation coefficients between zeta potentials of *Rhodococcus* cells and PDI values of metal NPs.

| *R. erythropolis* | Bi NPs | $Fe_2O_3$ NPs | Ni NPs | Co NPs | CuO NPs |
|---|---|---|---|---|---|
| IEGM 344 | 0,983 | −0,657 | 0,963 | 0,881 | −0,208 |
| IEGM 661 | −0,771 | −0,777 | −0,735 | −0,993 | −0,910 |
| IEGM 693 | 0,999 | 0,050 | 0,470 | −0,738 | 0,296 |
| IEGM 706 | 0,414 | 0,526 | 0,413 | 0,956 | 0,666 |
| IEGM 766 | 0,932 | 0,423 | 0,633 | 0,826 | −0,941 |
| *R. fascians* | | | | | |
| IEGM 173 | 0,572 | −0,719 | −0,485 | −0,153 | −0,444 |
| IEGM 525 | 0,367 | 0,093 | 0,073 | 0,696 | 0,842 |
| IEGM 531 | 0,998 | −0,393 | −0,639 | −0,612 | 0,035 |
| IEGM 534 | 0,628 | −0,282 | −0,710 | 0,900 | 0,051 |
| IEGM 1218 | 0,197 | 0,508 | 0,745 | 0,923 | 0,768 |
| *R. jostii* | | | | | |
| IEGM 60 | 0,136 | −0,761 | −0,773 | −0,895 | −0,740 |
| IEGM 68 | 0,538 | −0,425 | −0,508 | −0,749 | 0,781 |
| IEGM 458 | −0,672 | 0,911 | 0,774 | 0,925 | 0,576 |
| IEGM 508 | −0,612 | −0,068 | 0,128 | −0,672 | 0,060 |
| IEGM 550 | 0,919 | −0,217 | 0,966 | −0,345 | 0,707 |
| *R. rhodochrous* | | | | | |
| IEGM 757 | 0,298 | −0,887 | −0,094 | 0,472 | 0,674 |
| IEGM 1161 | 0,718 | 0,373 | −0,158 | 0,107 | −0,137 |
| IEGM 1162 | 0,533 | −0,887 | 0,094 | −0,941 | −0,351 |
| IEGM 1360 | −0,686 | 0,485 | −0,136 | −0,974 | 0,963 |
| IEGM 1362 | −0,463 | 0,817 | −0,204 | −0,984 | −0,647 |
| *R. ruber* | | | | | |
| IEGM 628 | −0,031 | −0,689 | −0,305 | −0,833 | 0,558 |
| IEGM 1121 | −0,592 | −0,786 | 0,203 | −0,984 | −0,550 |
| IEGM 1135 | 0,923 | 0,925 | −0,175 | −0,784 | 0.613 |
| IEGM 1217 | 0,986 | 0,748 | −0,172 | −0,601 | −0,149 |
| IEGM 1352 | −0,406 | −0,700 | −0,031 | −0,851 | −0,542 |

### 3.2. *Rhodococcus* cell viability upon the exposure to metal NPs

The cell viability in presence of different concentrations of metal and metal oxide NPs (Figure 3) indicated the relative *Rhodococcus* resistance to Bi, Co and Ni NPs and sensitivity to Cu and CuO NPs. In general, NPs at lower (0.001–0.01 g/L) concentrations had little effect on cell viability, but led to 50–80% inhibition of cells at higher (0.1–1.0 g/L) concentrations. However, in the presence of cobalt NPs, the viability of *Rhodococcus* ranged from 80-120% regardless of the concentration of nanoparticles. It should be noted that the excess of the viability values of biotic controls (>100%), most noticeable in *R. erythropolis*, may be due to fragmentation of the cellular mycelium into short rod-shaped cells, characteristic of the stationary growth phase, under the effect of metal NPs. Representatives of *R. jostii*, *R. rhodochrous* and *R. ruber* were more sensitive to metal NPs, while *R. erythropolis* and *R. fascians* showed higher resistance to nanometals. These findings supported the idea that toxic effects of NPs dependent on their concentrations and physicochemical properties [5]. Indeed, the maximum antibacterial effects were found at higher concentrations when metal NPs had greater negative charges and formed stable monodisperse suspensions (see Figures 2 and 3). Based on the present results, it would be possible to select appropriate (sublethal) concentrations of individual NPs for the cell functionalization of particular *Rhodococcus* species.

### 3.3. Effects of metal NPs on zeta potentials of Rhodococcus cells

According to Figure 4, native *Rhodococcus* cells had a negative zeta potential, ranging from −21 to −45 mV under the experimental conditions (10 mM $KNO_3$, pH 5.5–6). Representatives of *R. rhodochrous* and *R. ruber* had the largest negative cell charges (from −32 to −45 mV) with the lowest fluctuations in zeta potential values within the species. While *R. erythropolis*, *R. fascinans* and *R. josii* strains had less negative average charges (−32, −28 and −32 mV correspondingly) and more significant intraspecies heterogeneity. The addition of metal and metal oxide NPs had diverse effects on the zeta potential of *Rhodococcus* cells. In particular, at low (0.001–0.01 g/L) concentrations of Bi NPs, the zeta potential of *R. erythropolis*, *R. fascinans* and *R. ruber* moved to slightly less negative values, while the zeta potential of *R. rhodochrous* and *R. josii* moved to a more negative area. At a higher concentration (0.1 g/L), the charge of most *Rhodococcus* spp. cells approached the highest negative values, while the maximum concentration (1.0 g/L) of Bi NPs resulted in a less pronounced negative shift of zeta potentials compared to control cells. Similar changes in the zeta potential of *Rhodococcus* cells were revealed under the influence of Co, CuO, and $Fe_2O_3$ nanoparticles. At the same time, the interaction of *R. erythropolis*, *R. fascians*, and *R. ruber* cells with Ni NPs caused a gradual concentration-dependent decrease in the negative zeta potential, while some negative shifts for the charge of *R. jostii* and *R. rhodochrous* cells were detected at 0.01–0.1 g/L Ni NPs.

Interestingly, the curves of the zeta potential of pure nanoparticles and NP-treated *Rhodococcus* cells largely coincided, indicating similar concentration-dependent trends in Figure 4. It seemed that with increasing concentrations of NPs, zeta potential values of bacterial cells approached the zeta potential of NPs, thus suggesting the accumulation of nanoparticles on the cell surface. This hypothesis was statistically verified for each *Rhodococcus* strain and NPs of each metal (Supplementary material, Table S2). The experimental dependence $y = |\zeta_1 - \zeta_2|$ from $x = \lg C$ was processed by the least squares method of linear dependence $y = ax + b$, where $\zeta_1$ is a zeta potential of *Rhodococcus* cells, $\zeta_2$ is a zeta potential of NPs, $C$ is the concentration of NPs.

The parameters $a$ and $b$ were found, as well as the standard deviation $\sigma_a$ of parameter $a$. Further, four degrees of confirmation were established for the formulated hypothesis – from 0 (not confirmed at all) to 3 (fully confirmed) – according to the following rule: degree is 0 if $a > 0$ and $a - \sigma_a > 0$; degree is 1 if $a > 0$ and $a - \sigma_a \leq 0$; degree is 2 if $a \leq 0$ and $a + \sigma_a > 0$; the degree is 3 if $a \leq 0$ and $a + \sigma_a \leq 0$.

Thus, the hypothesis is confirmed if the dependence $y = ax + b$ is decreasing, i.e. $a \leq 0$. But $a$ is determined with an error (deviation), so the range $a \pm \sigma_a$ should be considered. Then four options arise: (0) the entire range is in the positive region, the hypothesis is not confirmed at all; (1) the middle of the range is positive, but the range captures the negative region, the hypothesis is possible, but unlikely; (2) the middle of the range is negative, but the range captures the positive region, the hypothesis is almost confirmed; (3) the entire range lies in the negative region, the hypothesis is fully confirmed.

If the degree of confirmation is 1, then two more sub-options can be formulated. If the positive part of the interval $a \pm \sigma_a$ is more than twice the negative part, then it should be assumed that the hypothesis is not confirmed. If such difference is less than two times, then it should be assumed that the errors (standard deviations) are too large and nothing definite can be said about the hypothesis. For example, too large errors were characteristic for *R. fascians* IEGM 525 and Ni NPs, *R. josti* IEGM 60 and Bi NPs, *R. josti* IEGM 458 and Bi NPs, *R. rhodochrous* IEGM 757 and Co NPs.

Similar sub-options can be formulated if the degree of confirmation is 2. If the negative part of the interval $a \pm \sigma_a$ is more than twice the positive part, then it should be assumed that the hypothesis is confirmed. If such difference is less than two times, then it should be assumed that the errors (standard deviations) are too large and nothing definite can be said about the hypothesis. For example, too large errors were characteristic for *R. erythropolis* IEGM 706 and Bi NPs, *R. erythropolis* IEGM 344 and CuO NPs, *R. fascians* IEGM 525 and Bi NPs, *R. jostii* IEGM 550 and Ni NPs, *R. rhodochrous* IEGM 1162 and Bi NPs, *R. ruber* IEGM 1135 and Co NPs.

The results of statistical testing of the hypothesis are given in Table 1. The degree of confirmation is indicated for each strain and NPs of each metal. As an example, four graphs containing the revealed experimental dependences and their linear approximation for four different degrees of

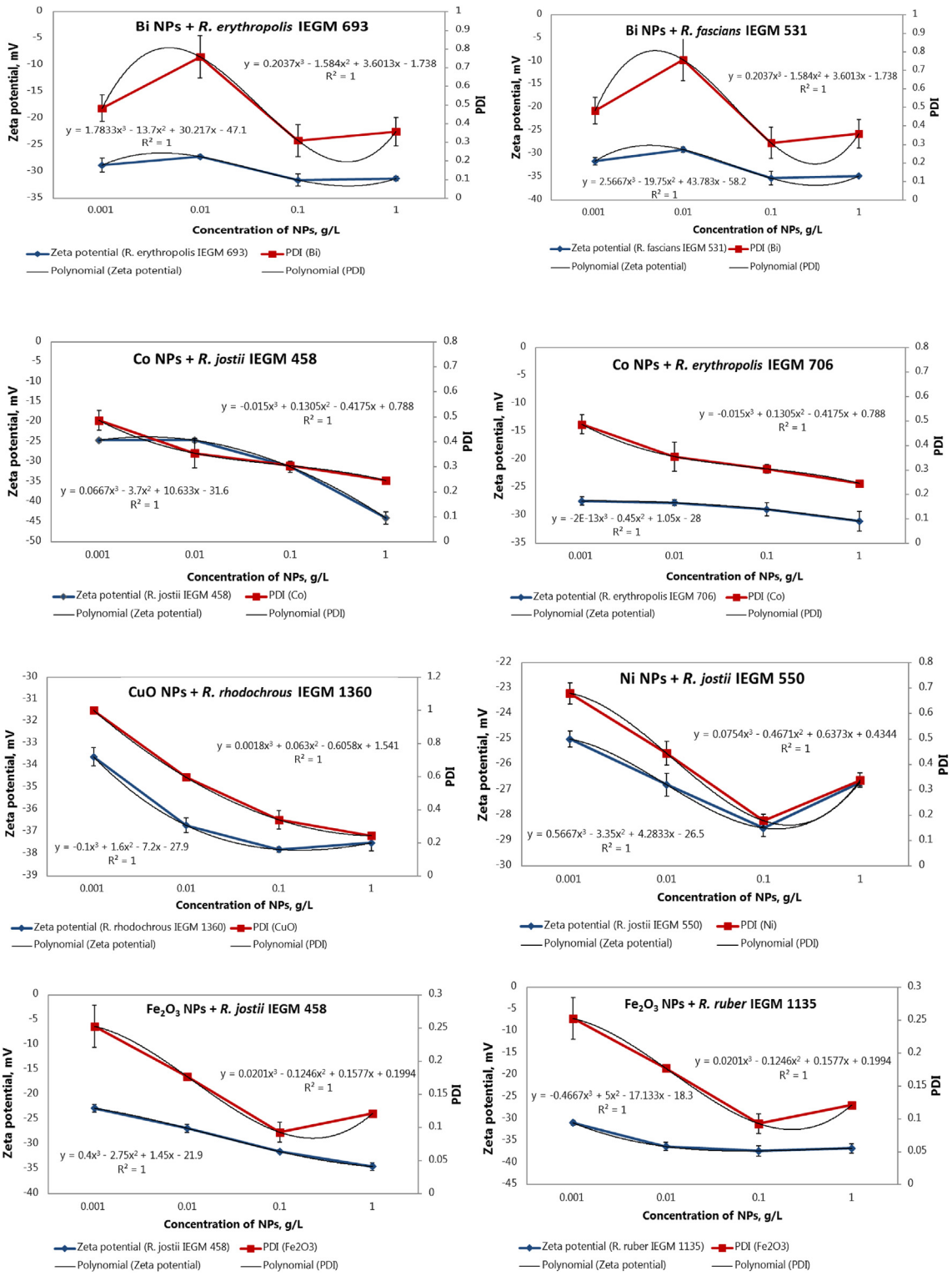


**Figure 6.** Correlation between the zeta potential of *Rhodococcus* cells and PDI values of metal NPs.

hypothesis confirmation are shown in the (Supplementary material, Figure S2). The physical meaning of the degree of confirmation of 0 is that the hypothesis is not confirmed at all: when the concentration of NPs increases, the zeta potential of bacterial cells differs more and more from the zeta potential of NPs, as illustrated for *R. fascians* IEGM 1218 cells and $Fe_2O_3$ NPs. Nevertheless, the hypothesis was statistically confirmed for a total 75% of *Rhodococcus* strains and metal NPs.

Using the results in Table 1, the studied *Rhodococcus* species were arranged according to the average degree of hypothesis confirmation in the following ascending row: *R. fascians* – 1.8; *R. erythropolis* – 2.2; *R. jostii* – 2.4; *R. ruber* – 2.7; *R. rhodochrous* – 2.8. Metal NPs were arranged according to the average degree of hypothesis confirmation in the following ascending row: Bi – 1.6; Ni – 2.48; Co – 2.48; $Fe_2O_3$ – 2.52; CuO – 2.7. Thus, based on the dynamics of zeta potential, it would be possible

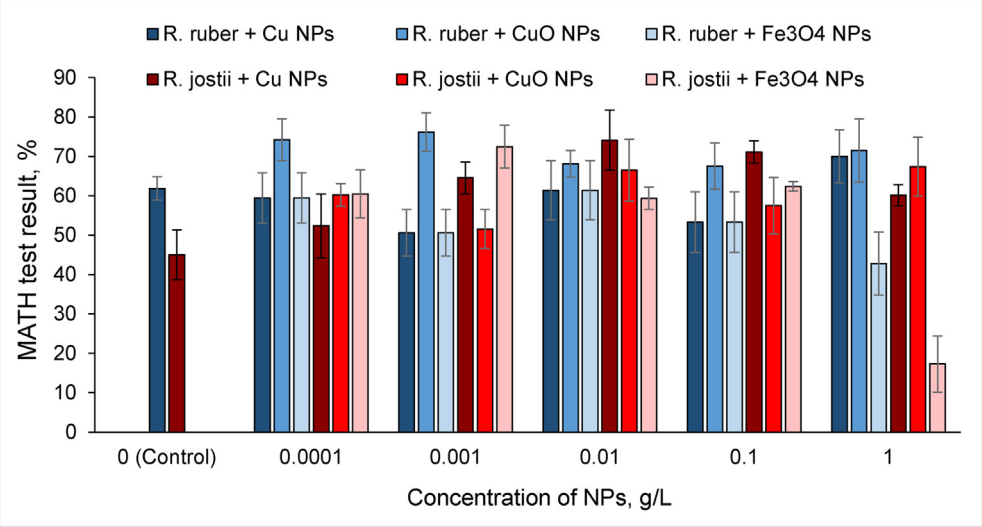


**Figure 7.** Effects of metal NPs on the *Rhodococcus* adhesion to *n*-hexadecane.

to predict the accumulation of metal NPs on the cell surface of particular *Rhodococcus* species. It seems that more toxic nanometals (e.g. CuO) accumulate more intensively on the bacterial cell wall than less toxic nanometals (Bi, Ni and Co). Other studies also reported the accumulation of metal NPs on the cell wall following its disintegration as the primary mechanism of toxicity [11]. Alternatively, the toxic metal accumulation on the cell surface can be considered as a mechanism of resistance since cell wall components or extracellular polymeric substances bind accumulated metal NPs, thus preventing their penetration to the cell membrane and cytoplasm [23, 24]. It is known that rhodococci are able to actively accumulate metal ions and use energy-dependent transport channels for the metal uptake and efflux [18], while the mechanisms of their interactions with metal nanoparticles remain unexplored.

To illustrate the accumulation of metal NPs on the bacterial cell surface, the AFM images of *Rhodococcus* cells incubated in the presence of nanoparticles are shown in Figure 5.

We further examined the correlation between PDI values of metal NPs and changes in zeta potential of *Rhodococcus* cells (Table 2). Interestingly, the correlation patterns between zeta potentials of bacterial cells and nanoparticle PDI values for several *Rhodococcus* strains (Figure 6) were highly similar to those revealed in the abiotic systems for metal NPs (Figure 2). At low concentrations (0.001–0.01 g/L), with an increase in the PDI of metal NPs, the zeta potential of *Rhodococcus* cells moved to a less negative area. While with an increase in the nanoparticle concentration and a corresponding decrease in their PDI to $\leq 0.5$, cellular zeta potentials shifted to larger negative values ($<-30$ mV). The revealed correlation between the surface charge of *Rhodococcus* cells and dispersity of metal NPs suggests that monodisperse nanoparticles interact more actively with bacterial cells due to their larger relative surface area, while the reactivity of NPs can be reduced by aggregation [25].

### 3.4. Effects of metal NPs on the adhesion of Rhodococcus cells to n-hexadecane

Cellular adhesion to *n*-hexadecane was measured for two *Rhodococcus* species to assess the effect of metal NPs on the cell surface hydrophobicity, an important physicochemical property that allows hydrocarbon-oxidizing bacteria to efficiently degrade a wide range of hydrophobic pollutants [17].

According to the MATH test (Figure 7), *R. ruber* IEGM 1121 cells demonstrated higher intrinsic adhesion to *n*-hexadecane compared to *R. jostii* IEGM 550, apparently due to the relative hydrophobicity of the cell wall. These findings are consistent with our previous and other group studies [9, 26] suggested the affinity of rhodococci to hydrophobic substrates.

The addition of metal and metal oxide NPs had diverse effects on the hydrophobicity of *Rhodococcus* cells. In particular, an increase in the adhesion of *R. jostii* cells to *n*-hexadecane was observed in the presence of increasing concentrations of Cu and CuO NPs. A similar but less pronounced increase in cell adhesion was recorded for *R. ruber* exposed to CuO NPs in the entire concentration range and Cu NPs only at the highest concentration (1 g/L). Conversely, treatment with $Fe_3O_4$ NPs resulted in a decrease in the adhesive activity of both *R. jostii* and *R. ruber* cells, especially at the highest concentration (1 g/L). There is only one report in the literature on the effect of metal nanoparticles on the surface hydrophobicity of microbial cells [27]. The authors proposed a new strategy to engineer a hydrophobic cell surface using the coating with gold NPs in order to increase the microbial adhesion at the air-water interface. The present results have shown that various nanometals can be used to modify the hydrophobic properties of *Rhodococcus* cells to increase their adhesion to hydrophobic or hydrophilic surfaces, which is especially important for obtaining an immobilized biocatalyst [28].

## 4. Conclusions

Diverse effects of transition metal and their oxide NPs on the viability, zeta potential and adhesion of *Rhodococcus* cells were revealed, depending on NP concentrations. With the NP concentration increase, the cellular zeta potentials become closer to NP values, thus indicating the accumulation of metal NPs on the bacterial cell surface. Whether such surface accumulation of nanometals enhances their toxic effect on bacteria or, conversely, is a protective mechanism of *Rhodococcus* cells that prevents NP internalization remains unclear and requires further investigation. It is also shown that nanometals in selected sublethal concentrations can be used to modify the electrical and hydrophobic properties of bacterial cells involved in adhesion, aggregation and other important physiological functions without adverse effects on their viability.

## Declarations

### Author contribution statement

Maria S. Kuyukina: conceived and designed the experiments, wrote and edited the paper.

Marina V. Makarova: performed the experiments, wrote and edited the paper.

Olga N. Pistsova and Grigorii G. Glebov: performed the experiments.

Mikhail A. Osipenko: analyzed and interpreted the data, wrote the paper.

Irena B. Ivshina: conceived and designed the experiments, edited the paper.

## Funding statement

This work was supported by the Ministry of of Science and Higher Education of the Russian Federation [AAAA-A20-120081990069-3, 122010800029-1], Russian Science Foundation [18-14-00140] and Russian Foundation for Basic Research [20-44-596001].

## Data availability statement

Data included in article/supp. material/referenced in article.

## Declaration of interest's statement

The authors declare no conflict of interest.

## Additional information

Supplementary content related to this article has been published online at https://doi.org/10.1016/j.heliyon.2022.e11632.

## References

[1] S.A. Hoang, L.Q. Nguyen, N.H. Nguyen, C.Q. Tran, D.V. Nguyen, N.T. Le, C.V. Ha, Q.N. Vu, C.M. Phan, Metal nanoparticles as effective promotors for Maize production, Sci. Rep. 9 (2019), 13925.

[2] E. Sánchez-López, D. Gomes, G. Esteruelas, L. Bonilla, A.L. Lopez-Machado, R. Galindo, A. Cano, M. Espina, M. Ettcheto, A. Camins, A.M. Silva, A. Durazzo, A. Santini, M.L. Garcia, E.B. Souto, Metal-based nanoparticles as antimicrobial agents: an overview, Nanomaterials 10 (2) (2020) 292.

[3] R. Deng, D. Huang, W. Xue, L. Lei, S. Chen, C. Zhou, X. Liu, X. Wen, B. Li, Eco-friendly remediation for lead-contaminated riverine sediment by sodium lignin sulfonate stabilized nano-chlorapatite, Chem. Eng. J. 397 (2020), 125396.

[4] T. Hirai, Y. Yoshioka, N. Izumi, K. Ichihashi, T. Handa, N. Nishijima, E. Uemura, K. Sagami, H. Takahashi, M. Yamaguchi, K. Nagano, Y. Mukai, H. Kamada, S. Tsunoda, K.J. Ishii, K. Higashisaka, Y. Tsutsumi, Metal nanoparticles in the presence of lipopolysaccharides trigger the onset of metal allergy in mice, Nat. Nanotechnol. 11 (2016) 808–816.

[5] L. Escorihuela, B. Martorell, R. Rallo, A. Fernández, Toward computational and experimental characterisation for risk assessment of metal oxide nanoparticles, Environ. Sci. J. Integr. Environ. Res.: Nano 5 (2018) 2241–2251.

[6] Y. Xu, C. Wang, J. Hou, P. Wang, G. You, L. Miao, Effects of cerium oxide nanoparticles on bacterial growth and behaviors: induction of biofilm formation and stress response, Environ. Sci. Pol. 26 (2019) 9293–9304.

[7] Y. Zhang, M. Yang, N.G. Portney, D. Cui, G. Budak, E. Ozbay, M. Ozkan, C.S. Ozkan, Zeta potential: a surface electrical characteristic to probe the interaction of nanoparticles with normal and cancer human breast epithelial cells, Biomed. Microdevices 10 (2) (2008) 321–328.

[8] E. Kłodzińska, M. Szumski, E. Dziubakiewicz, K. Hrynkiewicz, E. Skwarek, W. Janusz, B. Buszewski, Effect of zeta potential value on bacterial behavior during electrophoretic separation, Electrophoresis 31 (2010) 1590–1596.

[9] E.V. Rubtsova, M.S. Kuyukina, I.B. Ivshina, Effect of cultivation conditions on the adhesive activity of Rhodococcus cells towards n-Hexadecane, Appl. Biochem. Microbiol. 48 (2012) 452–459.

[10] S. Halder, K.K. Yadav, R. Sarkar, S. Mukherjee, P. Saha, S. Haldar, S. Karmakar, T. Sen, Alteration of Zeta Potential and Membrane Permeability in Bacteria: a Study with Cationic Agents 4, Springer Plus, 2015, pp. 672–686.

[11] Y.N. Slavin, J. Asnis, U.O. Häfeli, H. Bach, Metal nanoparticles: understanding the mechanisms behind antibacterial activity, J. Nanobiotechnol. 15 (2017) 65.

[12] S. Anuj, H. Gajera, D. Hirpara, B. Golakiya, The impact of bacterial size on their survival in the presence of cationic particles of nano-silver, J. Trace Elem. Med. Biol. 61 (2020) 126517–126524.

[13] M. Arakha, M. Saleem, B. Mallick, S. Jha, The effects of interfacial potential on antimicrobial propensity of ZnO nanoparticle, Sci. Rep. 5 (2015) 9578–9588.

[14] M. Bhagat, R. Anand, R. Datt, V. Gupta, S. Arya, Green synthesis of silver nanoparticles using aqueous extract of Rosa Brunonii Lindl and their morphological, biological and photocatalytic characterizations, J. Inorg. Organomet. Polym. Mater. 29 (2019) 1039–1047.

[15] A.S. Joshi, P. Singh, I. Mijakovic, Interactions of gold and silver nanoparticles with bacterial biofilms: molecular interactions behind inhibition and resistance, Int. J. Mol. Sci. 21 (20) (2020) 7658.

[16] C.A. Custódio, J.F. Mano, Cell surface engineering to control cellular interactions, ChemNanoMat 2 (5) (2016) 376–384.

[17] M.S. Kuyukina, I.B. Ivshina, Bioremediation of contaminated environments using *Rhodococcus*, in: H.M. Alvarez (Ed.), Biology of *Rhodococcus*. Microbiology Monographs vol. 16, Springer, Cham, 2019, pp. 231–270.

[18] A. Presentato, E. Piacenza, M. Cappelletti, R.J. Turner, Interaction of Rhodococcus with metals and biotechnological applications, in: H.M. Alvarez (Ed.), Biology of Rhodococcus. Microbiology Monographs vol. 16, Springer, Cham, 2019, pp. 334–357.

[19] M. Shinde, P. Salve, S. Rathod, Development and evaluation of nanoparticles based transdermal patch of agomelatine for the treatment of depression, J. Drug Delivery Therapeut. 9 (4-s) (2019) 126–144.

[20] R. Ragheb, U. Nobbmann, Multiple scattering effects on intercept, size, polydispersity index, and intensity for parallel (VV) and perpendicular (VH) polarization detection in photon correlation spectroscopy, Sci. Rep. 10 (2020), 21768.

[21] I.O. Korshunova, O.N. Pistsova, M.S. Kuyukina, I.B. Ivshina, The effect of organic solvents on the viability and morphofunctional properties of Rhodococcus, Appl. Biochem. Microbiol. 52 (2016) 43–50.

[22] M. Planchon, R. Ferrari, F. Guyot, A. Gélabert, N. Menguy, C. Chanéac, A. Thill, M.F. Benedetti, O. Spalla, Interaction between Escherichia coli and TiO2 nanoparticles in natural and artificial waters, Colloids Surf. B Biointerfaces 102 (2013) 158–164.

[23] N. Joshi, B.T. Ngwenya, C.E. French, Enhanced resistance to nanoparticle toxicity is conferred by overproduction of extracellular polymeric substances, J. Hazard Mater. 241–242 (2012) 363–370.

[24] V. Dunsing, T. Irmscher, S. Barbirz, S. Chiantia, Purely polysaccharide-based biofilm matrix provides size-selective diffusion barriers for nanoparticles and bacteriophages, Biomacromolecules 20 (10) (2019) 3842–3854.

[25] E.M. Hotze, J.-Y. Bottero, M.R. Wiesner, Theoretical framework for nanoparticle reactivity as a function of aggregation state, Langmuir 26 (13) (2010) 11170–11175.

[26] C.C. de Carvalho, L.Y. Wick, H.J. Heipieper, Cell wall adaptations of planktonic and biofilm Rhodococcus erythropolis cells to growth on C5 to C16 n-alkane hydrocarbons, Appl. Microbiol. Biotechnol. 82 (2) (2009) 311–320.

[27] Y. Kim, K. Jung, J. Chang, T. Kwak, Y. Lim, S. Kim, J. Na, J. Lee, I. Choi, L.P. Lee, D. Kim, T. Kang, Active surface hydrophobicity switching and dynamic interfacial trapping of microbial cells by metal nanoparticles for preconcentration and in-plane optical detection, Nano Lett. 19 (10) (2019) 7449–7456.

[28] A. Krivoruchko, M. Kuyukina, I. Ivshina, Advanced Rhodococcus biocatalysts for environmental biotechnologies, Catalysts 9 (3) (2019) 236.